

# 893. Experimental study of dynamic responses of casing deflection profile for blade rubbing classification

Lim Meng Hee<sup>1</sup>, Leong M. S.<sup>2</sup>

<sup>1</sup>Razak School of Engineering, Universiti Teknologi Malaysia, Malaysia

<sup>2</sup>Faculty of Mechanical Engineering, Universiti Teknologi Malaysia, Malaysia

E-mail: <sup>1</sup>mhlim@ic.utm.my, <sup>2</sup>salman.leong@gmail.com

(Received 07 August 2012; accepted 4 December 2012)

**Abstract.** Blade rubbing is one of the most destructive mechanical faults that frequently manifest in rotating machinery. Its occurrence is mainly caused by two distinctively different mechanisms and root causes, namely creep (elongated blades) and rotor eccentricity (diminished blade tip clearance). A successful classification of the types of blade rubbing is important as it could lead to identification of the root cause of the problem. This study explores a vibration method to classify blade rubbing based on the analysis of casing deflection profile. Different types of blade rubbing were simulated in an experimental rotor rig and vibration responses of the rotor casing under the influence of blade rubbing were measured and studied. Experimental results indicate that vibration characteristics of rotor casing change in accordance to different mechanisms of blade rubbing, resulting in fairly distinctive casing deflection profile. A quantitative method to classify blade rubbing was formulated based on the analysis of obtained results. A comparison made against the vibration spectrum analysis suggests that the analysis of casing deflection profile provides a more effective means to classify blade rubbing and therefore could be applied for detailed blade rubbing diagnosis in rotating machinery.

**Keywords:** casing, deflection, blade, rubbing, classification, diagnosis.

## Introduction

The occurrence of blade rubbing in rotating machinery has become more prevalent especially with the advent of high performance turbomachinery design. This is because the primary design consideration of these machines is to minimize the operational clearances between rotating blades and casing in order to increase cycle efficiencies and thereby reduce the overall fuel consumption [1]. The consequences of blade rubbing could be very serious as it can lead to other more destructive failures in machinery such as Foreign Object Damage (FOD) due to broken blade-parts. To date, abundant studies have been conducted to understand the effects and mechanisms of blade rubbing in rotating machinery. Choy [2] investigated the characteristics of the non-linear dynamics of rubbing and has established the relationship of various parameters of rubbing excitation such as the relationship of rub force and energy levels to rubbing duration and incidence separation angles. Laverty [3] studied the mechanics of rubbing between a compressor blade tip seals and rotor casing. He found that the total energy of rubbing is mainly contributed by the incursion rate of the rubbing as compared to rubbing velocity and the thickness of the blade. He concluded that the overall rubbing energy increased in proportion to the quantity of blades that are involved in the process of rubbing. Sawicki [4] studied the dynamic behavior of rotors rubbing and found that the vibration spectrum of rubbing is mainly dominated by sub-harmonic, quasi-periodic, and chaotic vibration components. Ahrens [5] conducted an experimental study to investigate the resulting contact forces (in radial and tangential direction) during the process of rubbing. Roques et al [6] formulated a mathematical rotor-stator model of a turbo-generator in order to study the speed transients and angular deceleration associated with rubbing. These reports, amongst others have provided a deeper understanding on the mechanics and mechanisms of rubbing and thus enabled a better interpretation of rubbing-based observations and signals in relation to its actual physical condition that occurred.

Blade rubbing detection in rotating machinery is often accomplished by establishing the vibration symptoms of rubbing from time domain (i.e. vibration waveform, orbit plot), frequency domain (i.e. FFT) and also time-frequency domain (i.e. wavelet and STFT) signal analysis. A literature review by Muszynska [7] provided exhaustive information related to vibration, rotor dynamics and the resulting rotor orbit during rubbing. This information could be used as a reference to detect blade rubbing in rotating machinery. Kubiak et al [8] highlighted that blade rubbing could be detected if the blade passing frequency (BPF) amplitude is found to be exceptionally high in the vibration spectrum. Besides this, the presence of the abnormal frequency harmonics peaks ( $2\times$ ,  $3\times$ ,  $4\times$ , etc.) of the operating speed in the vibration spectrum could also indicate the occurrence of blade rubbing. A drastic escalation in rotor sub-harmonic peaks in the vibration spectrum could also infer the presences of blade rubbing as reported by Meher-Homji [9]. Tejas [10] studied the early detection of rubbing in rotating machinery based on the vibration signal measured during a coast-up of a machine. He found that Hilbert–Huang signal analysis could be applied to detect early rubbing in a rotor system based on the vibration signal measured during the coast-up of a machine. Wavelet analysis method is also widely used to detect rubbing in rotating machinery. For instance, Peng [11] conducted a study to determine the effectiveness of using the conventional scalograms as compared to the reassigned scalograms for the detection of rubbing. He found that when rubbing occurred, its rubbing impacts could lead to an increase in vibration amplitude at high frequency region. He concluded that the vibration amplitude peaks of high frequencies region increase in correspondence to the increase of severity of rubbing. Wang [12] proposed a method to determine the location of rubbing in a rotor bearing system based on acoustics emission and wavelet analysis. Peng [13] used wavelet analysis as a mean for feature extraction of rubbing impact signal in a rotor system. Barzdaitis et al. [14] demonstrated an application of an optimized vibration monitoring and diagnostic system to detect rotor-to-stator rubbing in upper part of journal bearing of an industrial turbomachinery.

While wealth of reports revolve on the subject of blade rubbing detection based on various vibration signals analysis methods, specific vibration method to classify blade rubbing is not sufficiently addressed. The classification of the types of blade rubbing is important as it could lead to the identification of the root cause of the problem. Essentially, blade rubbing in rotating machinery is mainly caused by two distinctly different root causes namely, creep (elongated blade), hereafter referred to as creep rubbing, and the rotor eccentricity (diminished blade tip clearance), referred to as eccentricity rubbing (Fig. 1). Therefore, in order to rectify and prevent blade rubbing from recurring, different engineering approaches need to be undertaken in correspondence to the type of blade rubbing that occurred. For instance, in order to rectify and prevent creep rubbing from recurring, the blades that experience creep have to be replaced and the operational manner of the machine has to be altered in order to reduce the effect of irreversible thermal strain on the blades. On the other hand, in order to rectify eccentricity rubbing, the centerlines of rotor and casing have to be realigned. The difficulty to classify blade rubbing based on vibration spectrum analysis and its consequences of not being able to do so was experienced by the authors while undertaking a machinery troubleshooting task in one of the power stations in Malaysia. A brief chronology of the event is described as follows. One of the gas turbines in a local power station in Malaysia was experiencing erratic behavior in just three months after a scheduled overhaul. At the onset, blade rubbing was thought to be the prime suspect as some audible rubbing noises could be heard emanating from the compressor section during the coast down of the machine. Subsequently, steady state vibration signals of the gas turbine were measured at bearing location and the vibration spectrum revealed that the BPF amplitudes of certain stages of blades were found to be exceptionally high (10 folds of the normal amplitude value). On top of that, the vibration spectrum was also found to be dominated by peculiar vibration peaks which were not present in the vibration spectrum of a healthy gas turbine. Based on these observations, it is reasonable to deduce the potential occurrence of

blade rubbing in the machine. Despite that, the root cause of the blade rubbing could not be identified based on the pattern of the vibration spectrum. Under these circumstances, consensus on the rectification approach which need to be undertaken could not be achieved and consequently delaying the rectification works. This incident underlines the importance of blade rubbing classification as well as the need to formulate a vibration analysis method to achieve the objective.

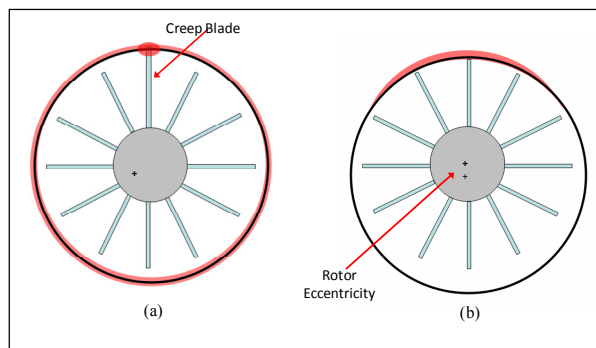


**Fig. 1.** Typical types of blade rubbing occurring in rotating machinery:  
(a) creep rubbing; (b) eccentricity rubbing

The solution approach hypothesized in this study is that rotating machinery that is subjected to different mechanisms of blade rubbing could result in fairly distinctive casing deflection profile. Blade rubbing classification can therefore be undertaken by analyzing the resulting casing deflection profile. Thus, this study attempts to shed light onto the following questions:

- What is the casing deflection profile of a machine that is under the influence of different mechanisms of blade rubbing namely creep and eccentricity based ones?
- Can casing deflection profile be employed effectively to classify the types of blade rubbing?
- Is casing deflection profile analysis a better method than the vibration spectrum analysis to achieve the objective of the study?

## Experimental Study

An experimental rig was fabricated and installed in the laboratory (Fig. 2) in an attempt to study the effects of different mechanisms of blade rubbing on the vibration characteristics of a rotor casing. The experimental rig consists of a rotor and casing, twelve pieces of blades, and some experimental control mechanisms that were designed and fabricated. The mechanical parameters which were controlled in this study include blade length (to simulate creep), blade tip clearance (to simulate rotor eccentricity) and rubbing severity. Various lengths of blades were fabricated to represent normal blades (153 mm) and creep blade conditions (155 mm and 157 mm). The initial blade tip clearance (measured from blade tip to inner surface of casing) was designed to be 7 mm. The casing deflection profile of a baseline (healthy) condition was measured based on the condition that the rotor was fitted with blades of normal length to achieve an uniform blade tip clearance. In order to examine the vibration response of creep blade, the healthy blade was simply replaced with a longer blade. Meanwhile, in order to create creep rubbing condition, a component termed as “top-head” (see Fig. 3a) made of aluminum sheet metal was used to extend the blade length and to act as the rubbing medium between the blade and the casing. Meanwhile, rotor eccentricity condition (or the impending stage rub) was induced in the experiment by reducing the blade tip clearance. This was achieved by dropping the upper casing in the vertical direction using "eccentricity setter" (see 3b). Eccentricity setters

are tiny pieces of sheet metal each with 1 mm thickness placed between the upper and lower casing. Thus, to introduce rotor eccentricity in vertical direction, the eccentricity setters were simply removed to achieve the intended drop. In this study, the initial blade tip clearance of 7 mm was reduced to only 2 mm to represent rotor eccentricity or the condition of impending rub. Subsequently, eccentricity rubbing condition was created by fitting top-head onto each and every blade to rub against the casing. In this experimental study, all vibration signals were measured under steady state condition with the operational speed of the rotor set to 1200 RPM. Accelerometers were attached to the rotor casing in tri-axes using a magnetic block and was intended to be used as the roving point to generate the resulting casing deflection profile. There were a total of 7 roving points (P1 to P7) located along the curvature of the rotor casing (refer to Fig. 4). In addition, one extra accelerometer (P8) was also placed at the bearing housing to be used as the reference point. IMC Data Acquisition Box (DAQ) was used to acquire the vibration signals of the experimental study.

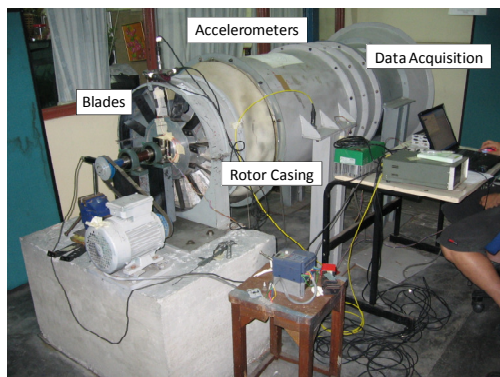


**Fig. 2.** Experimental rig and set up

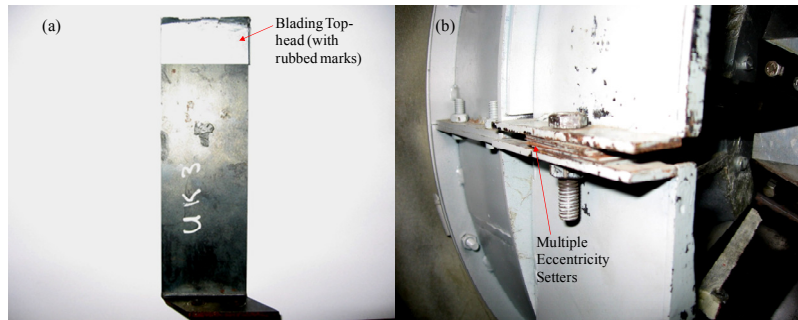


**Fig. 3.** Experiment control mechanisms: (a) blading top-head with rubbed marks; (b) multiple eccentricity setters placed between upper and lower casing

### Casing Deflection Profile Analysis

The dynamics deflection profile of a rotor casing under the influence of blade rubbing could be established based on the concept of Operational Deflection Shape (ODS). Essentially, ODS represents the relative motion of a machine or a structure under the actual forced excitation. ODS analysis provides a feasible technique to investigate the dynamic responses of a machine under the actual excitation force. This method is the most useful in situations where the actual force that acts on the system could not be easily measured such as for large industrial machines (i.e. gas turbine) and engineering structures (i.e. bridges). In the industry, ODS method has been

successfully used to detect myriad of machinery problems such as rotor imbalance and misalignment ([15], [16]), amongst other.

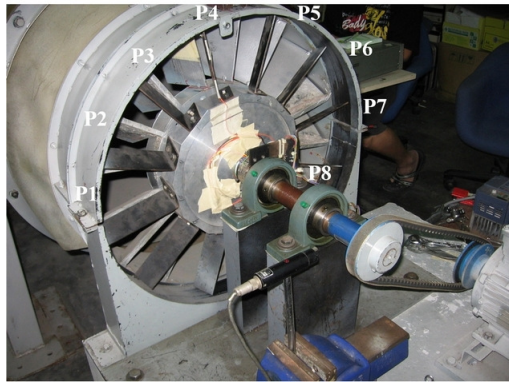


**Fig. 4.** Locations of measurement (P1-P7) on rotor casing and bearing housing (reference point, P8)

An ODS is defined in magnitude and phase values for each vibration response (also known as a degree of freedom (DOF)) on a test machine. Generally, this requires that either all vibration responses are measured simultaneously or that they are measured under conditions that can guarantee their correct magnitudes and phases relative to one another. Simultaneous measurement requires a multi-channel acquisition system that can simultaneously acquire all responses. While, a sequential acquisition requires that a fixed reference response to be acquired and that cross channel measurements to be calculated between it and other roving responses. For sequential ODS measurement, the underlying assumption is that the operating condition of a machine does not change between the different measurement sequences and therefore a calculation of the cross-power spectra between each DOF and the reference point is sufficient to characterize the relative movement of the machine under test. The cross-power spectrum,  $G_{xy}(\omega)$  is defined in Eq. (1) as:

$$G_{xy}(\omega) = F_x(\omega)F_y^*(\omega) \quad (1)$$

where  $F_x(\omega)$  is the Fourier spectrum of a measured response of a DOF and  $F_y^*(\omega)$  denotes the complex conjugate of the Fourier spectrum of the measured fixed reference response. In order to evaluate the changes of the casing deflection profile due to blade rubbing, two numerical assessment methods, namely the Shape Correlation Coefficient (SCC) and Shape Percentage Difference (SPD) are studied.

#### a) Shape Correlation Coefficient (SCC)

SCC is a numerical calculation that measures the similarity between two complex vectors. SCC is defined in Eq. (2):

$$SCC = \frac{\|ODS_F \bullet ODS_B^*\|^2}{\|ODS_F\| \|ODS_B\|} \quad (2)$$

$ODS_B$  represent the baseline ODS of a machine in healthy condition. And the  $ODS_F$  represents the ODS of the machine in faulty condition.  $ODS_B^*$  denotes the complex conjugate of the  $ODS_B$ . The symbols of  $\bullet$  and  $\| \cdot \|$  represent the dot product of two vectors and the

magnitude square of the vector, respectively. *SCC* is a normalized dot product between the ODS in test and the baseline (healthy) ODS. It has a value between 0 and 1. A value of 1 indicates that the ODS has not changed. As a rule of thumb, *SCC* value greater than 0.90 indicates a strong correlation between the shapes of two vectors. A value less than 0.50 generally indicates that a considerable change in the ODS shape has been detected. As such, the *SCC* method provides a single numerical number to measure the changes in shape of an ODS.

#### **b) Shape Percentage Difference (*SPD*)**

In contrast, *SPD* does not only measure the changes in the shape of the vectors, but also considers the changes in amplitude of the ODS. *SPD* is defined in Eq. (3):

$$SPD = \frac{|ODS_F - ODS_B|}{|ODS_B|} \quad (3)$$

Similarly,  $ODS_B$  and  $ODS_F$  represent the baseline ODS and faulty ODS of the machine respectively. While  $||$  represents the magnitude of the vector. A *SCC* value of near to 1 and a *SPD* value of near to 0 signify that the ODS in test is unchanged relative to the baseline ODS. On the other hand, a small *SCC* value and a large *SPD* values indicate otherwise. The effectiveness of *SCC* and *SPD* methods as an indicator to detect the severity of blade rubbing is examined in this paper.

### **Experimental Results**

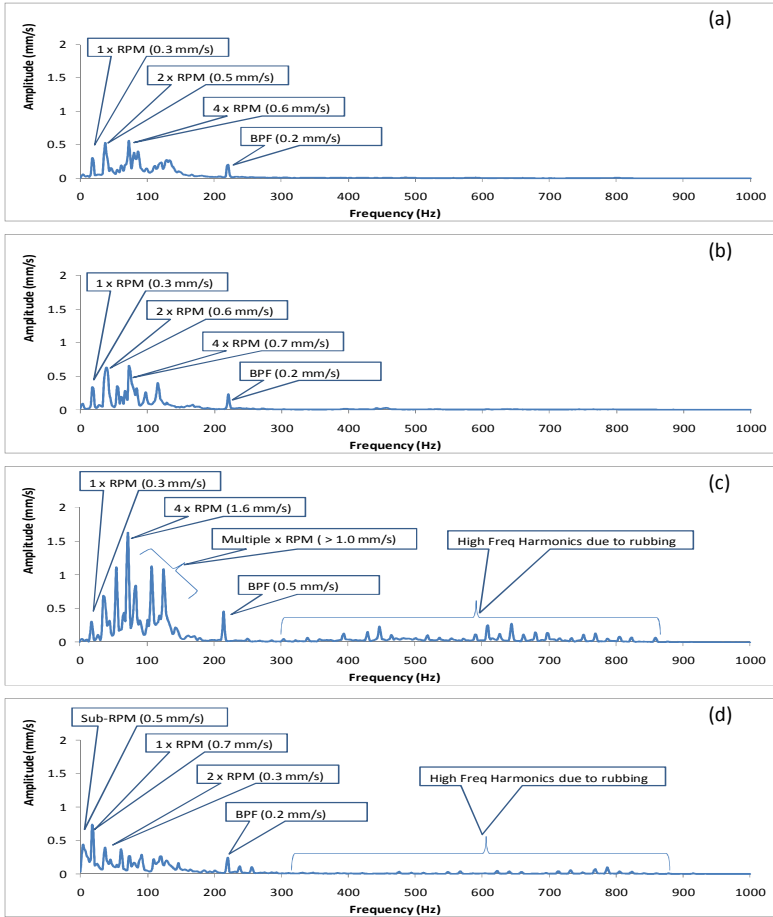
#### **a) Vibration Spectrum Analysis**

Fig. 5 illustrates the frequency spectrum of bearing vibration for baseline and various faulty conditions studied in this paper. By comparing the vibration spectrum of rotor eccentricity (impending rub) condition (Fig. 5b) to the baseline condition (Fig. 5a), no significant changes in its vibration pattern could be observed that could help to indicate the fault. However, when eccentricity rubbing condition (Fig. 5c) was induced in the experiment, substantial changes in the vibration spectrum could be observed as compared to the baseline condition. The huge escalation of the amplitude of  $\times 2$  to  $\times 6$  rpm components could be readily observed. Besides, an abundance of abnormally high peaks at the region of 300 Hz to 850 Hz is also present in the vibration spectrum. These phenomena do not appear for both the vibration spectrum of baseline and rotor eccentricity condition (impending rub) and are consistent to the typical vibration characteristics found for blade rubbing in rotating machinery. While for creep rubbing condition, some increment in the amplitude of  $\times 1$  rpm component (from 0.3 mm/s to 0.5 mm/s) could be observed. Besides, an abundance of vibration peaks around 300 Hz - 850 Hz could also be observed in its vibration spectrum albeit in relatively smaller magnitude as compared to the eccentricity rubbing condition. These phenomena also provide indication about the presence of minor blade rubbing in the rotor system. Although vibration spectrum is a feasible method to detect and compare the severity of blade rubbing (by comparing the amplitude of its vibration peaks), information pertaining to the physical mechanism of blade rubbing could not be easily drawn from the pattern of the vibration spectrum. As a result, blade rubbing classification based on vibration spectrum analysis could not be easily achievable.

#### **b) Casing Deflection Profile Analysis**

Dynamic movement of rotor casing under the influence of blade rubbing is considered in this section. Fig. 6 illustrates the resulting casing deflection profile for baseline and various faulty conditions studied in this paper. These casing deflection profiles represent the vibration responses of a rotor casing at the forcing frequency of 217 Hz, which corresponds to the blade passing frequency of the experimental rig. The casing deflection profile on the left and right of

Fig. 6 illustrate the movement of the rotor casing in expansion and contraction modes respectively. The amplitudes and relative phase angle for all DOF are tabulated in Table 1.



**Fig. 5.** Vibration spectra of various experimental conditions: (a) baseline; (b) rotor eccentricity; (c) eccentricity rubbing; (d) creep rubbing

**Table 1.** Amplitude and phase angle for all the DOFs of various experimental conditions

Experimental Conditions		Measurement Points (DOF)						
		P1	P2	P3	P4	P5	P6	P7
Baseline (Healthy)	Amp (mm/s)	0.5	1.2	0.5	0.2	1.1	1.3	0.6
	Phase (°)	7	4	10	9	6	6	12
Rotor Eccentricity	Amp (mm/s)	0.1	0.4	0.3	1.3	0.1	0.1	0.4
	Phase (°)	70	296	320	177	327	299	80
Eccentricity Rubbing	Amp (mm/s)	0.2	1.4	0.5	2.2	0.9	1.3	1.4
	Phase (°)	59	213	92	85	123	194	104
Creep Rubbing	Amp (mm/s)	0.5	2.3	1.1	0.9	0.1	2.0	0.4
	Phase (°)	106	341	162	156	99	345	138

Fig. 6a illustrates the casing deflection profile of the experimental rig at baseline condition. It is observed that all DOFs measured along the curvature of the upper rotor casing expand and contract (back and forth) in fairly synchronized manner and with reasonably consistent phase

angle to each other. From Table 1, the largest movement was found at point 2 (1.2 mm/s) and point 6 (1.3 mm/s) among all DOFs of the rotor casing. These DOFs points represent the DOFs of the rotor casing in diagonal axes (which is about 45° from x or y axis). While the smallest movement was observed at point 4 (0.2 mm/s) in the DOF aligns with the vertical y axis. These observations show that under baseline condition, the largest movement of the rotor casing took place in the most flexible planes on the diagonal axes, while the smallest movement observed in vertical y axis was restricted by the fastening mechanism emplaced in vertical and horizontal axes of the experimental rig. At a glance, the casing deflection profile of the baseline condition resembles a flattened semi-circle.

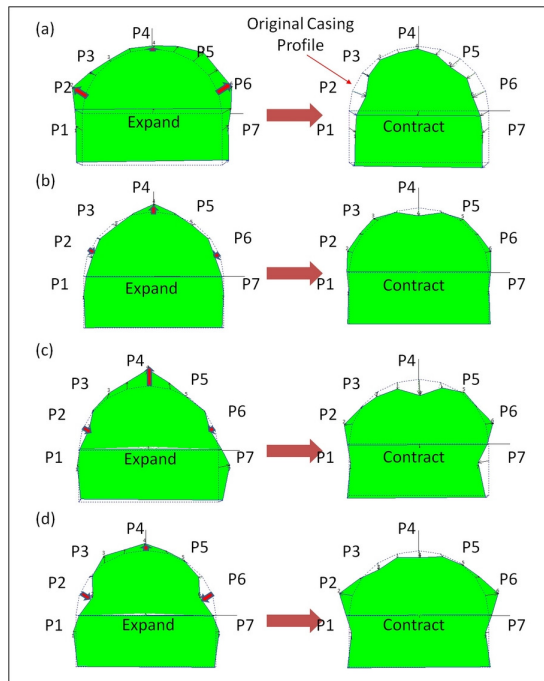


**Fig. 6.** Casing deflection profile for (a) baseline; (b) rotor eccentricity; (c) eccentricity rubbing; (d) creep rubbing. Pictures on the right and left represent the rotor casing in expansion and contraction modes respectively

Subsequently, when rotor eccentricity (impending rubbing) condition was induced in the experiment, its casing deflection profile changed from a flattened semi-circle to a shape of a protuberance or a bulge in expansion mode (see Fig. 6b). In contrast, the largest movement was observed at point 4 (1.3 mm/s) in the vertical y axis as compared to the diagonal planes under baseline condition. In close examination, as the rotor casing in full expansion mode, some contraction (inverse in direction) at points 2 and point 6 in diagonal axes could be observed and this phenomena were not detected for baseline condition. This observation suggests that when rotor eccentricity condition occurs, a great amount of air pressure builds up in the interior of casing (due to diminished blade tip clearance) leading to casing deflection profile that resembles a bulge.

Next, the casing deflection profile of eccentricity rubbing is shown in Fig. 6c. At a glance, the casing deflection profile of the eccentricity rubbing resembles the shape of that rotor eccentricity condition albeit relatively larger in size. The largest movement for eccentricity rubbing condition was also observed to be located at point 4 (2.2 mm/s) in vertical y axis, coinciding to the location of rubbing on the casing. The vibration amplitude of point 4 in y axis

was found to be double of amplitude of rotor eccentricity condition. Some contraction in movement for point 2 and 6 in diagonal axes was also noticeable, which is consistent with the rotor eccentricity condition. Therefore, analysis of the casing deflection profile could provide some useful evidence about the evolution of the blade rubbing from the impending rub to eccentricity rubbing condition.

Lastly, the casing deflection profile of creep rubbing is studied. From Fig. 6d, the casing deflection profile of creep rubbing is found to possess some common features found from both baseline and eccentricity rubbing conditions. Firstly, the casing deflection profile of creep rubbing in expansion mode shows contracting movement at point 2 and point 6 in diagonal axes (albeit in much larger amplitude) which is similar to the casing deflection profile of eccentricity rubbing. Secondly, by comparing the amplitude of all DOFs of the rotor casing, the largest movement for creep rubbing is found to be located at points 2 and point 6 in diagonal axes and the smallest movement is measured at point 4 in vertical  $y$  axis, which is similar to the characteristics of rotor casing of baseline condition. This observation suggests that in the event of creep rubbing the overall blade tip clearance remained unchanged and the only rubbing that occurred is mainly caused by the creep blade once per revolution. The impact of creep rub therefore resembles the mechanism of an impulsive excitation that allows the rotor casing to deform freely at its most flexible axes (diagonal planes) as seen at point 2 and 6. This is opposed to eccentricity rubbing, whereby rubbing occurred continuously for every running blade in one revolution. The unique characteristics of both blade rubbing conditions could hold the key to differentiate them and is discussed in the following section.

## Discussion

### a) Blade Rubbing Detection and Severity Assessment

In order to detect blade rubbing based on casing deflection profile, the *SCC* and *SPD* methods were used. A fault is detected if a casing deflection profile differs significantly from the baseline condition. As a rule of thumb, a *SCC* value of smaller than 0.9 ( $SCC < 0.9$ ) and a *SPD* value of larger than 0.5 ( $SPD > 0.5$ ) could indicate the presence of faults. Fig. 7 shows the *SCC* and *SPD* values for the experimental conditions studied in the experiment. The *SCC* values for rotor eccentricity, eccentricity rubbing, and creep rubbing were calculated to be 0.1375, 0.3220, and 0.2559 respectively. These *SCC* numbers indicate that the casing deflection profile of these conditions was found to significantly differ from the baseline condition. Meanwhile, the *SPD* values of the rotor eccentricity, eccentricity rubbing, and creep rubbing were calculated to be 0.9545, 2.2787, and 1.1615 respectively. In other words, the casing deflection profile of the eccentricity rubbing condition has changed 227 % from the baseline condition and therefore is the most severe fault among these faulty conditions. Besides this, *SPD* values also indicate that the severity of eccentricity rubbing is approximately two times of rotor eccentricity and creep rubbing conditions. While both *SCC* and *SPD* values are found to be a good indicator to detect blade rubbing, *SPD* possess the added advantage to enable the estimation of the blade rubbing severity.

### b) Blade Rubbing Classification and Diagnosis

From the experimental results, it is evident that when blade rubbing occurs, the casing deflection profile changes in accordance to the excitation mechanisms of blade rubbing. In order to classify blade rubbing based on casing deflection profile, a polar representation of the amplitude and phase angle of these selected critical points (e.g. point 2 and point 6 in diagonal axes and point 4 in vertical  $y$  axis) is proposed. Fig. 8 illustrates the polar plots of the selected critical points for all experimental conditions of this study. In baseline condition, the vector of points 2 and point 6 (diagonal axes) and the vector of point 4 in vertical  $y$  axis was observed to be located close to each other with fairly consistent phase angle. The polar plot also reveals that the largest amplitude is found in both point 2 and point 6 in diagonal axes (see Fig. 8a). For

rotor eccentricity condition, the phase angle between points in diagonal axes and point in vertical axis has changed considerably to about  $120^\circ$  with the largest amplitude shifted from diagonal axes to point 4 in vertical  $y$  axis. The changes in phase angle between diagonal and vertical axes and the shift of the dominating axis could indicate fault has been developed in the rotor system. For eccentricity rubbing, the phase angle between vertical to diagonal points has widened to approximately  $180^\circ$  with the largest vibration amplitude seen at vertical  $y$  axis (see Fig. 8d). The reverse of phase angle between diagonal and vertical point indicates the occurrence of blade rubbing. For creep rubbing, the polar plot indicates that the phase angle between vertical and diagonal points is also found to be approximately  $180^\circ$ . This confirmed that when blade rubbing occurs, the reverse of phase angle of  $180^\circ$  between diagonal to vertical axes is evident. In order to differentiate creep rubbing from eccentricity rubbing, analysis of the amplitude ratio between vertical and diagonal points could be used and the results are listed in Table 2. The amplitude ratio of larger than 1 indicates that the dominating vibration axis is located in vertical axis and thus attributable to rotor eccentricity induced rubbing, while the amplitude ratio of smaller than 1 indicates that the dominating axis is in diagonal axes and thus attributable to creep induced blade rubbing. The study of the relationship of phase angle and the amplitude ratio for these selected critical points provides a mean to classify blade rubbing faults.

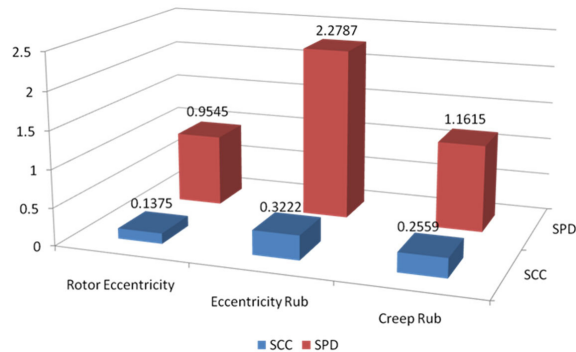


Fig. 7. SCC and SPD for various experimental conditions

Table 2. Amplitude ratio of selected critical DOF (vertical axis to diagonal axes) of experimental conditions

Experimental Conditions	Vibration Amplitude (mm/s)		
	Diagonal Axes (Average)	Vertical Axis	Amp Ratio (Vertical Axis / Diagonal Axes)
Rotor Eccentricity	0.3	1.3	5.1
Eccentricity Rubbing	1.4	2.2	1.6
Creep Rubbing	2.1	0.9	0.4

### c) Quantitative Method for Blade Rubbing Classification and Diagnosis

Fig. 9 illustrates the quantitative method for blade rubbing classification based on casing deflection profile analysis. In summary, SPD analysis provided the first screening test to evaluate the overall condition of the rotor based on the changes of the rotor casing deflection relative to the baseline condition. In this case, the SPD value is not only applicable to detect blade rubbing fault but also provides an indication about the severity of the faults. Subsequently, a combination of polar plot, and the amplitude ratio calculation between the selected critical points located in diagonal axes and vertical axis of the resulting casing

deflection profile could be employed for blade rubbing classification. A relatively consistent phase angle between diagonal and vertical axes could indicate that the rotor system is still in healthy condition. A shift in phase angle between diagonal and vertical axes in a quantum larger than  $90^\circ$  could indicate that fault has developed in the rotor system that has significantly altered the casing deflection profile. Subsequently, a phase angle of approximately  $180^\circ$  between points located in diagonal and vertical axes indicates the occurrence of blade rubbing. An amplitude ratio of the critical points (in vertical axis and diagonal axes) of larger than 1 ( $> 1$ ) indicates the occurrence of eccentricity rubbing, while the amplitude ratio of smaller than 1 ( $< 1$ ) indicates the presence of creep rubbing. This quantitative method has provided a unified and step by step approach to detect, classify and diagnose the root cause of blade rubbing, which is not achievable based on the conventional vibration spectrum analysis.

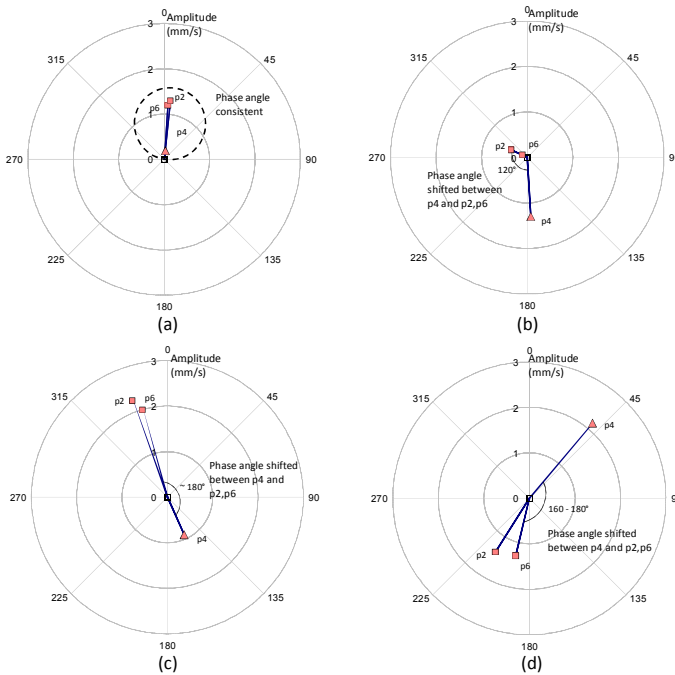


**Fig. 8.** Polar plots of the selected critical DOFs: (a) consistent phase angle for baseline condition; (b) phase angle between P4 and P2, P6 has changed substantially for rotor eccentricity; phase angle between P4 and P2, P6 has shifted  $180^\circ$  for creep rubbing (c) and eccentricity rubbing (d)

**d) Some Recommendations and Generalization of Findings**

**i.** Some unique characteristics of casing deflection profile under the influence of different mechanisms of blade rubbing were observed in the experimental study. When rotor eccentricity (impending rub) condition occurs, a great amount of air pressure is built up in the rotor casing due to diminished blade tip clearance. This results in a change of casing deflection profile that resembles a bulge in the direction corresponding to the location of impending blade rubbing. In the event of eccentricity rubbing, a continuous forcing excitation exerted by each running blade onto the adjacent casing caused the largest movement being observed at the point of rub and resulted in a shape of an enlarged bulge. As a result the exact location of rub on the casing could reasonably be estimated based on the largest deflection amplitudes measured along the circumference of the rotor casing. In contrast, the location of rubbing excitation as exerted by creep blade is constantly in motion coincides with the rotational cycle of the rotor system.

Therefore, no fixed location of rubbing on the casing shall be identified in the event of creep rubbing.

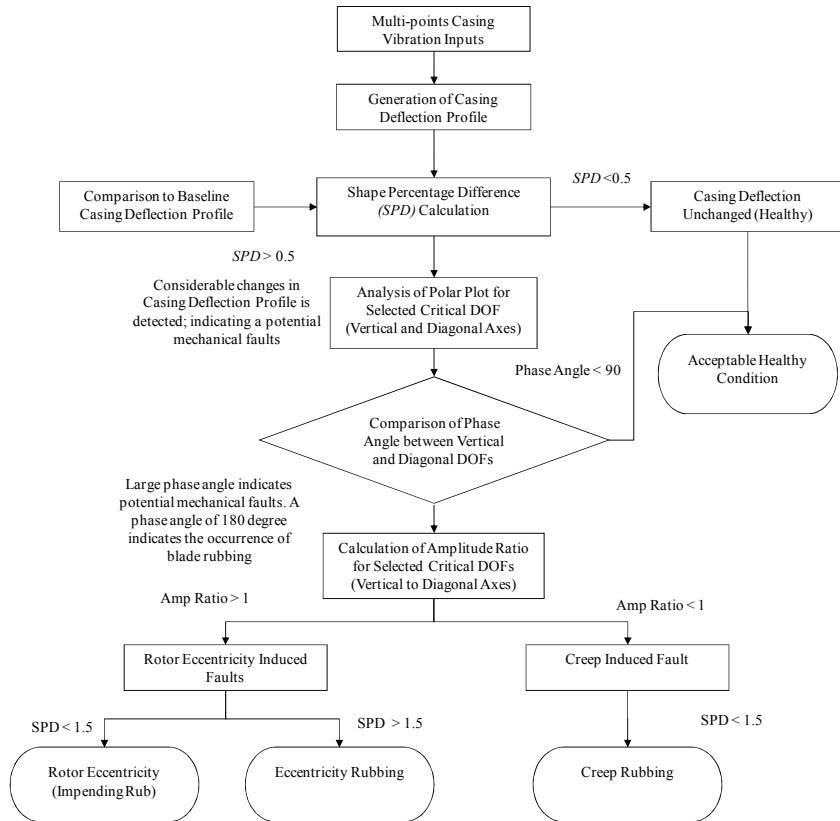


Fig. 9. Quantitative method for blade rubbing classification and diagnosis

ii. Rotor eccentricity condition is a precursor for the massive eccentricity blade rubbing to occur. An early detection of the rotor eccentricity condition is therefore important to machinery operator as this would allow a minor rectification work to be undertaken in time avoiding more serious consequences. Based on the experimental results, rotor eccentricity condition could not be readily detected based on vibration spectrum analysis. In contrast, the proposed casing deflection profile was found to be a more feasible method to detect this condition based on the appreciable changes observed in the casing deflection profile.

iii. To date, bearing vibration measurement is still represents the most widely employed method when it come to detect and diagnose blade rubbing in rotating machinery. However, this study suggests that multi-point casing vibration measurements (casing deflection profile) could be a more effective method to detect, classify and diagnose the root cause of blade rubbing. Therefore, casing vibration measurement shall be conducted whenever possible in lieu of bearing vibration for more detailed blade rubbing analysis in rotating machinery.

## Conclusions

Some unique vibration characteristics of the casing deflection profile under the influence of different mechanisms of blade rubbing were detected experimentally and explained. It was

found that the resulting casing deflection profile could be used for blade rubbing classification and root cause diagnosis purposes. A quantitative method to classify blade rubbing was also formulated. A comparison made against the conventional vibration spectrum analysis method has demonstrated the advantages of the proposed method for blade rubbing classification and diagnosis in rotating machinery. In addition, the proposed method is also found to possess an added advantage to detect the elusive rotor eccentricity condition prior to the occurrence of blade rubbing.

## Acknowledgements

This work is supported by UTM Research University Grant (GUP) scheme entitled 'A Proposed Standard for Wavelet-Based Condition Monitoring by Formulating Unique Fingerprint Specific for Machine' (Q.J.13000.7140.01.J88), financed by Ministry of Higher Education (MOHE) of Malaysia.

## References

- [1] **Turner K. E., Michael Dunn, Corso Padov** Airfoil deflection characteristics during rub events. *ASME Journal of Turbomachinery*, Vol. 134, Issue 1, 2012, p. 011018-1 - 011018-8.
- [2] **Choy F. K., Padovan J.** Non-linear transient analysis of rotor-casing rub events. *Journal of Sound and Vibration*, Vol. 113, Issue 3, 1987, p. 529 - 545.
- [3] **Laverty W. F.** Rub energetics of compressor blade tip seals. *Wear*, Vol. 75, Issue 1, 1982, p. 1 - 20.
- [4] **Sawicki J. T., Padovan J., Al-Khatib R.** The dynamics of rotor with rubbing. *International Journal of Rotating Machinery*, Vol. 5, 1999, p. 295 - 304.
- [5] **Ahrens J., Ulbrich H., Ahaus G.** Measurement of contact forces during blade rubbing. *Proceedings of IMechE*, Paper No. C576/083/2000, 2000, p. 259 - 263.
- [6] **Roques S., Legrand M., Cartraud P., Stoisser C., Pierre C.** Modeling of a rotor speed transient response with radial rubbing. *Journal of Sound and Vibration*, Vol. 329, Issue 5, 2010, p. 527 - 546.
- [7] **Muszynska A.** Rotor-to-stationary element rub-related vibration phenomena in rotating machinery – literature survey. *Shock & Vibration Digest*, Vol. 21, 1989, p. 3 - 11.
- [8] **Kubiak J., Gonzalez G., Garcia G., Urquiza B.** Hybrid fault pattern for the diagnosis of gas turbine component degradation. *Proceedings of JPGC'01 – International Joint Power Generation Conference*, New Orleans, Louisiana, June 4-7, 2001, paper no: PWR-19112.
- [9] **Meher-Homji C. B.** Blading vibration and failures in gas turbines: Part B – Compressor and turbine airfoil distress. *ASME Turbo Expo*, 1995, paper no. 95-GT-419.
- [10] **Tejas H. P., Ashish K. D.** Study of coast-up vibration response for rub detection. *Mechanism and Machine Theory*, Vol. 44, Issue 8, 2009, p. 1570 - 1579.
- [11] **Peng Z. K., Chu F., Tse P. W.** Detection of the rubbing-caused impacts for rotor-stator fault diagnosis using reassigned scalogram. *Mechanical Systems and Signal Processing*, Vol. 19, Issue 2, 2005, p. 391 - 409.
- [12] **Wang Q., Chu F.** Experimental determination of the rubbing location by means of acoustic emission and wavelet transform. *Journal of Sound and Vibration*, Vol. 248, Issue 1, 2001, p. 91 - 103.
- [13] **Peng Z. K., He Y., Lu Q., Chu F.** Feature extraction of the rub-impact rotor system by means of wavelet analysis. *Journal of Sound and Vibration*, Vol. 259, Issue 4, 2003, p. 1000 - 1010.
- [14] **Barzdaitis V., Bogdevičius M., Didžiokas R.** Diagnostics procedure for identification of rubs in rotor bearings. *Journal of Vibroengineering*, Vol. 12, Issue 4, 2010, p. 552 - 565.
- [15] **Surendra N. Ganeriwala, Brian Schwarz, Richardson M. H.** Operational deflection shapes to detect unbalance in rotating equipment. *Sound and Vibration Magazine*, May 2009, p. 11 - 13.
- [16] **Surendra N. Ganeriwala, Zhuang Li, Richardson M. H.** Using operational deflection shapes to detect misalignment in rotating equipment. *Proceedings of IMAC XXVI*, February 4-7, 2008.